Nuclear Engineering and Technology 52 (2020) 661–673

Contents lists available at ScienceDirect

Nuclear Engineering and Technology

journal homepage: www.elsevier.com/locate/net

Original Article

Simulations of BEAVRS benchmark cycle 2 depletion with MCS/CTF coupling system

Jiankai Yu, Hyunsuk Lee, Hanjoo Kim, Peng Zhang, Deokjung Lee*

Department of Nuclear Engineering, Ulsan National Institute of Science and Technology, 50 UNIST-gil, Ulsan, 44919, South Korea

ARTICLE INFO

Article history:
Received 5 February 2019
Received in revised form
27 August 2019
Accepted 17 September 2019
Available online 18 September 2019

Keywords:
MCS/CTF
MCS/TH1D
BEAVRS cycle 2
Quarter-core depletion

ABSTRACT

The quarter-core simulation of BEAVRS Cycle 2 depletion benchmark has been conducted using the MCS/CTF coupling system. MCS/CTF is a cycle-wise Picard iteration based inner-coupling code system, which couples sub-channel T/H (thermal/hydraulic) code CTF as a T/H solver in Monte Carlo neutron transport code MCS. This coupling code system has been previously applied in the BEAVRS benchmark Cycle 1 full-core simulation. The Cycle 2 depletion has been performed with T/H feedback based on the spent fuel materials composition pre-generated by the Cycle 1 depletion simulation using refueling capability of MCS code. Meanwhile, the MCS internal one-dimension T/H solver (MCS/TH1D) has been also applied in the simulation as the reference. In this paper, an analysis of the detailed criticality boron concentration and the axially integrated assembly-wise detector signals will be presented and compared with measured data based on the real operating physical conditions. Moreover, the MCS/CTF simulated results for neutronics and T/H parameters will be also compared to MCS/TH1D to figure out their difference, which proves the practical application of MCS into the BEAVRS benchmark two-cycle depletion simulations.

1. Introduction

With the increase of computational capability and the requirements of Monte Carlo neutron transport, the CORE (Computational Reactor Physics and Experiment Laboratory) group at UNIST (Ulsan National Institute of Science and Technology) has been developing the Monte Carlo neutron transport code – MCS [1], which is designated for application in full-core fuel-pin-wise analysis with high fidelity especially for large scale LWRs (light water reactors), other than a reference tool of benchmark testing for deterministic neutronic codes. The sub-channel T/H (thermal/hydraulic) code CTF [2] and the steady-state fuel performance prediction code FRAPCON [3] have been fully coupled within MCS source code to construct the Monte Carlo based multi-physics coupling code system via a cycle-wise Picard coupling scheme and the PDTS interface (Pin-wise Data Transfer Scheme) [4–6].

Other multi-physics coupling code systems are also being developed worldwide. In the CASL (The Consortium for Advanced Simulation of Light Water Reactors) project [7], the BEAVRS benchmark has been simulated by the VERA (Virtual Environment for Reactor Applications) code system for depletion of both Cycle 1 and 2 with multi-physics feedback [8]. VERA [9–11] is a set of comprehensive computational tools and supporting infrastructure in LWR modelling and simulations, which consists of the deterministic neutronic code MPACT [12], sub-channel T/H code CTF, the fuel performance code BISON [13] and so on. In addition, based on the Monte Carlo neutronic code, RMC [14] has been coupled with COBRA-EN and CTF respectively [15,16], and the full core depletion simulation of BEAVRS Cycle 1 and 2 with T/H feedbacks has been performed. Recently, the updated results for Cycle 2 depletion simulation has been accomplished by the newly developed RMC/CTF coupling code system [17,18].

Previously, the quarter core simulation for the BEAVRS Cycle 1 depletion with T/H feedback has been performed using MCS/TH1D and MCS/CTF coupling code systems [19]. This paper will focus on the application of the MCS/CTF coupling code system to BEAVRS Cycle 2 depletion with T/H feedback. Meanwhile, the results simulated by MCS/TH1D will also be presented and discussed. Section 2 of this paper introduces certain methodologies and techniques of the MCS based N-T/H (neutronic-thermal/hydraulic) coupling scheme. Section 3 describes the BEAVRS Cycle 2 depletion benchmark and its computational conditions; Section 4 describes

* Corresponding author.
E-mail address: deokjung@unist.ac.kr (D. Lee).

https://doi.org/10.1016/j.net.2019.09.007

the numerical results from the MCS/CTF simulation, a comparison with the measured data and a discussion of the difference in the results between MCS/CTF and MCS/TH1D. Finally, Section 5 summaries this work, draws conclusions based on the simulation results and outlines the future work.

2. Methodologies

The coupling scheme and corresponding index mapping technique are described in this section.

2.1. MCS-based N-T/H coupling schemes

The MCS-based N-T/H inner-coupling scheme adopts the cycle-wise Picard iteration coupling scheme, (see Fig. 1 flowchart). Thus, all T/H simulation codes (either CTF or TH1D) are compiled into a static library and coupled with MCS source code via a pin-wise data transfer scheme (PDTS), which means that the coupled T/H simulation code is considered as a T/H solver providing T/H feedback into the Monte Carlo neutron transport solver.

As shown in Fig. 1, the T/H standalone solvers (TH1D or CTF) receive the power distribution tallied from the N^{th} cycle (including inactive and active cycles) of Monte Carlo (MC) neutron transport. After the simulation of T/H standalone solver is finished, fuel temperatures, coolant temperatures and densities are collected and fed back into the MC transport to update the nuclide number densities and material temperatures of fuel and coolant. After this update, the $(N+1)^{th}$ cycle of MC neutron transport is ready to run. This N-T/H iteration is repeated until both neutronic and T/H behaviors have converged. Once all MC cycles are finished, both neutronic and T/H quantities are collected to obtain the statistics of all tallied results, including fuel temperature, coolant temperature and density.

2.2. Features of pin-wise data transfer scheme

PDTS (Pin-wise Data Transfer Scheme) is the coupling interface implemented in MCS code to couple other feedback solvers, including T/H and fuel performance solvers. The power exchanged from MCS to T/H solve is the pin-averaged value with axial distribution. However, the fuel temperature from T/H solver back into MCS has intra-pellet profile. Considering the different meshes in the radial direction of heat conduction model for fuel pellet, the mesh-dependent pellet temperature should be averaged and then feedback into MCS. By default, CTF divides fuel pellet into 10 equal-interval radial meshes, whereas 10 equal-area rings are set as radial mesh in TH1D. However, the same axial mesh division has been applied in both CTF and TH1D, which make it easier to realize the index-mapping between MCS and T/H solvers for both fuel pins and coolant channels. Moreover, the coolant temperature and density transferred from CTF should be averaged over the surrounded 4 subchannels and then mapped to a pin in MCS. The detailed formula for the average of fuel temperature and coolant temperature are described in the reference paper [6]. Unlikely, TH1D treats the surrounded 4 quarter of subchannel as the closed single coolant channel. Therefore, the MCS/TH1D can provide pin-wise distribution for T/H quantities in the fuel assembly or core level simulation. The difference lies on that CTF is capable of dealing with cross-flow effects among neighbouring subchannels.

2.3. Index mapping techniques for refueling

Since the default index numbering used in the MCS and T/H solvers are different, index mapping is one of the most important components in the PDTS interface to ensure that the exchange of full core pin-wise power distribution and T/H distribution data takes place correctly, both for axial and radial distributions. The detailed technique used in MCS-based multiphysics coupling system is described in the reference paper [6]. However, the assembly refueling (or shuffling) from End of Cycle 1 to Beginning of Cycle 2 should be also taken into account in the index mapping, which is also presented in Appendix I. Note that the assembly rotation caused by shuffling the loading pattern takes effects in the index mapping. Particularly, in the case of quarter core symmetry modelling, the shuffled fuel assembly should be rotated according to the symmetry boundary condition, which is mirror in this work.

2.4. Xenon treatment

The equilibrium xenon model has been implemented in MCS

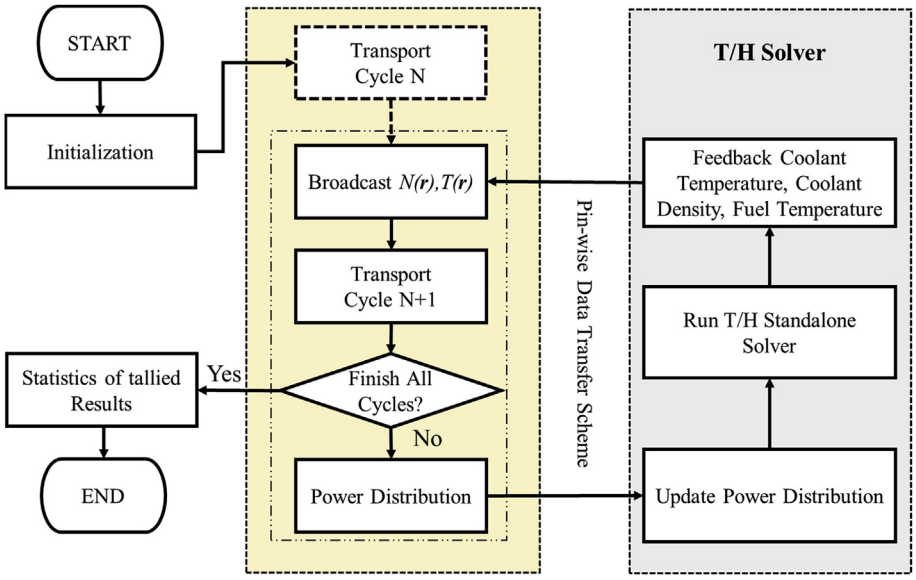

Fig. 1. Flow chart of MCS/CTF coupling interface.

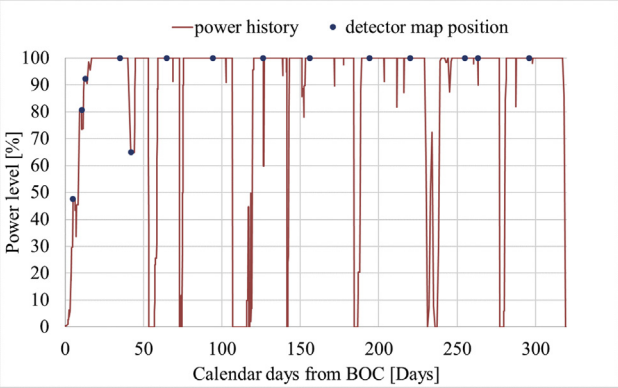

Fig. 2. Power history of BEAVRS Cycle 2.

Table 1
T/H boundary condition.

Parameters [unit]	Values
Relative Power [%]	100.00
Outlet Pressure [MPa]	15.513
Inlet mass flow rate [kg/s]	17083.33
Inlet Temperature [°C]	292.70
Gap conductance [W/(m^2·K)]	10000.00

code to reduce the Xenon oscillation phenomenon, which is caused by the combination of statistical uncertainty from Monte Carlo method, and large neutron absorption cross sections characteristics of Xenon itself [19]. To be brief, at the beginning of each cycle of Monte Carlo neutron transport, the flux together with macroscopic reaction rates tallied from previous Monte Carlo transport cycle will be used to update Xenon number density according to the equilibrium Xenon number density calculation formula, which has been described in detail in the reference paper [19].

3. Benchmark description

As Cycle 1 depletion has been simulated elsewhere, this section discusses BEAVRS Cycle 2 depletion only.

3.1. Benchmark description

The BEAVRS benchmark was released in 2013 [20], and revised in 2016 [21] and 2018 [22], respectively. The current version is 2.0.2, with core loadings and detector signals from the realistic nuclear power plant for the first two cycles of operation. More details (on full core geometry, fabricated fuel assembly loadings, burnable absorber pin layouts, operational histories, control rod positions, and boron concentration), can be referred to in the benchmark manual. The detailed power history of Cycle 2 depletion is shown in Fig. 2. Table 1 lists the T/H boundary conditions through the whole fuel cycle.

3.2. Computational conditions

A total of 15 time-steps are set in the depletion simulation. For example, 100% power level at each following 0.00, 0.31, 3.01, 27.02, 33.48, 50.19, 76.05, 96.13, 124.25, 155.09, 183.43, 207.55, 222.47, 248.06, 257.00 EFPDs (effective full power days). For each steady state nutronic simulation of all the burnup steps, 40 inactive and 40 active batches or multi-cycles ("multi-cycle" is the keyword in MCS input to indicate the number of cycles in each batch) are simulated. Note that Batch Method [23] has been implemented in MCS to get the fission source distribution converged quickly by reducing the inter-cycle correlation in Monte Carlo neutron transport. Each batch contains 300 single cycles, each single cycle including 10,000 histories. These parameters are identical to the calculation parameters used in the previous BEAVRS benchmark simulation with MCS.

For these calculation parameters, the statistical uncertainty of tallied pin-wise flux is less than 1% for the quarter core model. The eight T/H feedbacks are performed every 10 batches of Monte Carlo neutron transport to guarantee that the statistical uncertainties of tallied power density for the quarter core between two successive T/H conductions are globally low enough.

Additionally, measurement conditions for the Cycle 2 depletion are listed in Table 2. Those measurement conditions (including power level, inlet coolant temperature, and control rod bank position) are used in the MCS restarting calculation to obtain the simulated CBC (criticality boron concentration) results based on the depleted material composition from depletion simulation. Note that the time step in the depletion is displayed in the "Burnup" column of Table 2.

3.3. Refueling from cycle 1 to cycle 2

The assembly layouts at Cycle 1 and 2 and the corresponding rotation angle for the shuffling of spent fuels are illustrated in Tables 3–5, respectively. Note that the assembly name "NEW" stands for the fresh fuel in the Cycle 2 fuel loading. The other terms are spent fuels reloaded from the Cycle 1 depletion. This

Table 2
Measurement condition.

Step	Burnup [EFPD]	Power [%]	Inlet Temperature [K]	Control Rod Bank Position			
				A	B	C	D
1	0.31	29.11	564.414	228	228	228	221
2	3.01	80.47	565.358	228	228	228	177
3	5.39	99.99	566.719	228	228	208	202
4	27.02	99.68	566.636	228	228	228	215
5	33.48	65.00	564.497	228	228	228	177
6	50.19	100.16	567.053	228	228	228	220
7	76.05	99.90	567.275	228	228	228	210
8	96.13	100.08	566.956	228	228	228	211
9	124.25	99.75	566.956	228	228	228	211
10	155.09	99.91	567.164	228	228	228	212
11	183.43	99.96	567.206	228	228	228	210
12	207.55	99.55	566.928	228	228	228	211
13	222.47	99.91	567.247	228	228	228	210
14	248.06	99.92	566.914	228	228	228	217

Table 3
Assemblies layout of BEAVRS Cycle 1.

H01	G01	F01	E01	–	–	–	–
H02	G02	F02	E02	D02	C02	–	–
H03	G03	F03	E03	D03	C03	B03	–
H04	G04	F04	E04	D04	C04	B04	–
H05	G05	F05	E05	D05	C05	B05	A05
H06	G06	F06	E06	D06	C06	B06	A06
H07	G07	F07	E07	D07	C07	B07	A07
H08	G08	F08	E08	D08	C08	B08	A08

Table 4
Assemblies layout of BEAVRS Cycle 2.

NEW	NEW	NEW	F05				
C03	D02	E02	NEW	NEW	G06		
A06	D05	NEW	F03	C02	NEW	F07	
G08	E01	G04	NEW	H05	B03	NEW	
F01	D03	NEW	D04	NEW	C06	NEW	E06
B07	G01	H03	NEW	D07	NEW	B05	NEW
A08	G02	A07	C04	A05	E04	B04	NEW
B06	A08	B07	F01	H07	A06	C03	NEW

Table 5
Rotation angle of BEAVRS Cycle 2.

0	0	0	90				
180	90	0	0	0	180		
180	180	0	90	0	0	180	
0	180	90	0	0	0	0	
90	0	0	0	0	270	0	270
90	90	0	0	270	0	0	0
90	180	270	0	180	180	270	0
90	180	180	180	180	270	0	0

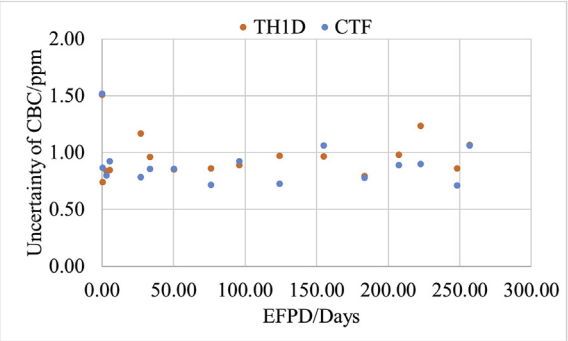

Fig. 3. Uncertainty of CBC at each burnup step of Cycle 2.

information is utilized in MCS/CTF and MCS/TH1D coupling simulations to construct the mapping matrix via index mapping techniques. The angle values in Table 5 is in units of degree in the clockwise direction.

4. Results and discussions

The results of Cycle 2 depletion with different T/H feedbacks are presented in this section.

4.1. Convergence behaviour

To display the convergence in the whole Cycle 2 depletion simulations, Fig. 3 shows the uncertainty of simulated CBC from MCS/CTF and MCS/TH1D coupling at each burnup step.

As shown in Fig. 3, the uncertainties of CBC lie within the range of approximately 0.7 ppm–1.5 ppm during the whole Cycle 2 depletion, so the convergence behavior in eigen-values can be proved.

Table 6
Results of computation time.

Step #	Burnup [EFPD]	Computation Time [hours]		Time Ratio
		TH1D	CTF	
0	0.00	7.56	11.65	1.54
1	0.31	9.55	13.02	1.36
2	3.01	10.01	12.52	1.25
3	5.39	10.18	12.64	1.24
4	27.02	10.29	12.68	1.23
5	33.48	10.39	12.50	1.20
6	50.19	10.42	12.64	1.21
7	76.05	10.42	12.38	1.19
8	96.13	10.52	12.12	1.15
9	124.25	10.55	12.04	1.14
10	155.09	10.61	12.97	1.22
11	183.43	10.75	12.84	1.19
12	207.55	10.80	12.26	1.14
13	222.47	10.76	12.69	1.18
14	248.06	10.77	12.99	1.21
15	257.00	10.70	12.83	1.20
Total	N/A	164.27	200.77	1.22

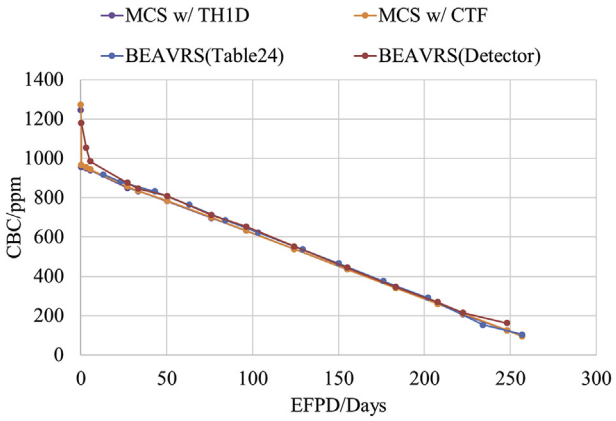

Fig. 4. CBC letdown of BEAVRS Cycle 2 depletion.

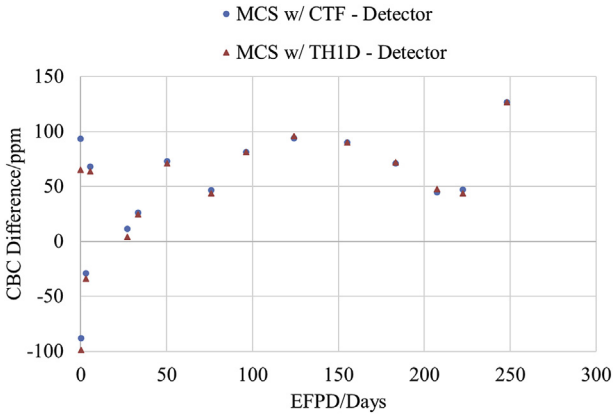

Fig. 5. CBC difference swing with BEAVRS Cycle 2 depletion.

4.2. Depletion results

4.2.1. Simulation time

The simulation time of MCS/TH1D and MCS/CTF coupling

Table 7
CBC data comparison for Cycle 2.

Step	Measured [ppm]	MCS/TH1D [ppm]	Difference (TH1D) [ppm]	MCS/CTF [ppm]	Difference (CTF) [ppm]
1	1180	1093.94 ± 0.79	−86.06	1149.04 ± 0.69	−30.96
2	1054	981.87 ± 1.09	−72.13	1004.63 ± 0.79	−49.37
3	985	955.92 ± 0.84	−29.08	953.80 ± 0.76	−31.20
4	876	867.38 ± 0.85	−8.62	884.74 ± 0.92	8.74
5	846	842.81 ± 1.17	−3.19	863.99 ± 0.73	17.99
6	809	793.39.±0.96	−15.61	810.67 ± 0.87	1.67
7	712	707.99 ± 0.85	−4.01	721.31 ± 0.94	9.31
8	653	643.83 ± 0.86	−9.17	652.85 ± 0.86	−0.15
9	552	546.86 ± 0.89	−5.14	559.25 ± 0.95	7.25
10	445	444.74 ± 0.97	−0.26	453.87 ± 0.93	8.87
11	346	348.08 ± 0.97	2.08	356.13 ± 1.21	10.13
12	270	272.03 ± 0.79	2.03	276.11 ± 1.27	6.11
13	215	220.36 ± 2.05	5.36	224.83 ± 1.30	9.83
14	137	137.93.±1.24	0.93	146.29 ± 1.75	9.29

systems are listed in Table 6. The results show the simulation time at each burnup step and the total time of BEAVRS Cycle 2 depletion. Based on this comparison of time ratio, CTF costs more time than TH1D by 14% (Step 9 and 12) to 54% (Step 0). Overall, the average time ratio is approximately 22%.

4.2.2. CBC results

The CBC results at HFP (Hot Full Power) of BEAVRS Cycle 2 depletion is obtained by MCS/CTF and MCS/TH1D coupling simulations, respectively. The results in Fig. 4 show that both MCS/TH1D and MCS/CTF can get considerably good CBC results in comparison to the measured data in Table 24 and the detector signals in the BEAVRS user manual [20–22]. Their differences are also illustrated in Fig. 5, where the discrepancy of CBC lie within the range from −100 ppm to 100 ppm, except for the last measurement point (127 ppm difference at 248.06 EFPD). Six of them are located within ±50 ppm. It can be concluded that the results calculated from MCS/TH1D and MCS/CTF agree well at the whole Cycle 2 lifetime. Note that the calculation condition of MCS simulation (100% Hot Full Power) is different from the measurement condition.

4.3. Comparison with measurement

4.3.1. CBC results

The CBC results at realistic operating condition of Cycle 2 depletion in MCS were obtained by restarting the calculation based

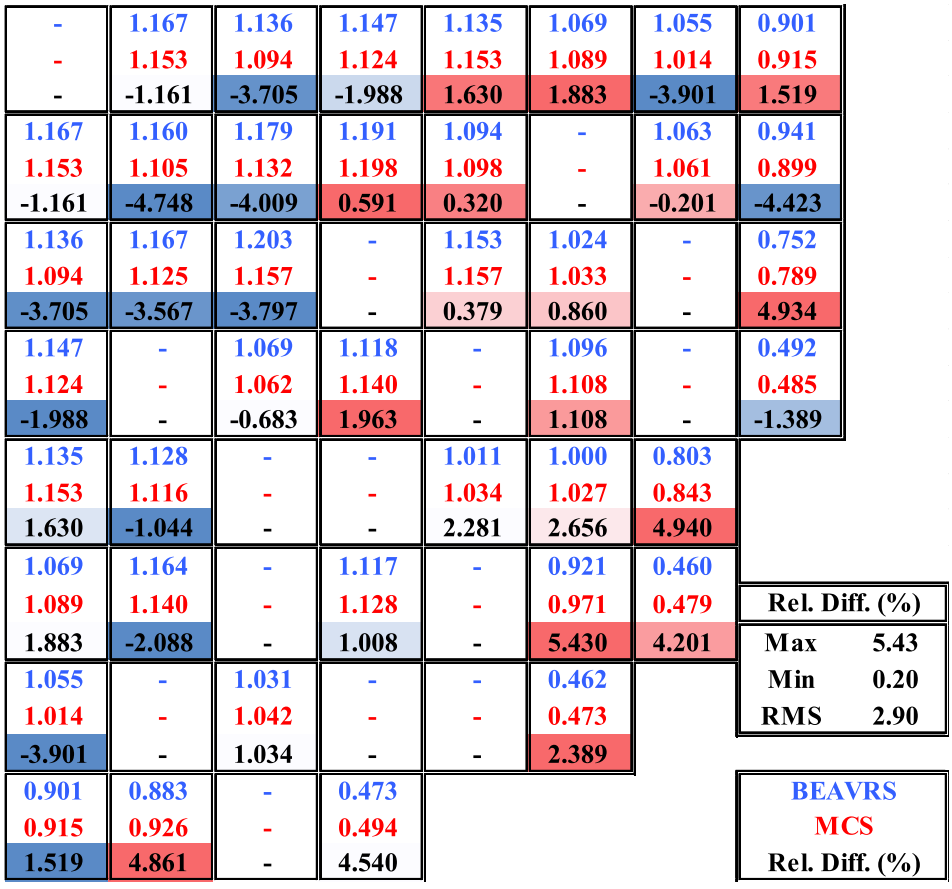

Fig. 6. Assembly-wise detector signals distribution at BOC of Cycle 2 (Step 3).

-	1.051	1.047	1.068	1.120	1.037	1.019	0.814
-	1.045	1.060	1.072	1.121	1.033	0.999	0.838
-	-0.600	1.224	0.376	0.089	-0.384	-1.955	2.896
1.051	1.048	1.090	1.179	1.088	-	-	0.843
1.045	1.054	1.098	1.207	1.092	-	-	0.842
-0.600	0.619	0.771	2.373	0.372	-	-	-0.177
1.047	1.090	1.213	-	1.229	1.064	-	0.741
1.060	1.105	1.227	-	1.237	1.051	-	0.741
1.224	1.340	1.181	-	0.642	-1.265	-	0.029
1.068	-	1.077	1.255	-	1.188	-	0.533
1.072	-	1.054	1.247	-	1.190	-	0.525
0.376	-	-2.155	-0.666	-	0.145	-	-1.442
1.120	1.093	-	-	1.148	1.065	0.814	
1.121	1.102	-	-	1.165	1.045	0.824	
0.089	0.797	-	-	1.457	-1.888	1.210	
1.037	1.156	-	1.200	-	0.914	0.506	
1.033	1.156	-	1.172	-	0.914	0.499	
-0.384	0.012	-	-2.344	-	-0.043	-1.330	
1.019	-	1.056	-	-	0.516		
0.999	-	1.044	-	-	0.493		
-1.955	-	-1.148	-	-	-4.433		
0.814	0.828	-	0.523				
0.838	0.834	-	0.530				
2.896	0.673	-	1.281				

Rel. Diff. (%)	
Max	4.43
Min	0.01
RMS	1.47

BEAVRS
MCS
Rel. Diff. (%)

Fig. 7. Assembly-wise detector signals distribution at MOC of Cycle 2 (Step 9).

on the depletion dependent materials composition, which was previously stored from the depletion simulations. Then, the real operating condition parameters are applied in the restarting calculation. The real measurement condition, including burnup, power level, inlet coolant temperature, and the position of the control rod bank are listed in Table 2. Table 7 tabulates the boron letdown curve data at each Cycle 2 burnup step.

The reference paper [24] lays out criteria for accuracy of high-fidelity simulations of the BEAVRs benchmark. It is stated that HFP CBC comparisons should be within 25 ppm, and that axially integrated detector flux root mean square error (RMSE) should be less than 1.5%. This paper adopts 25 ppm as the acceptable CBC results and 10 ppm as the good CBC results. However, the criteria for axially integrated flux is relaxed a little bit considering the Monte Carlo statistical uncertainty and the computation consumption (both CPUs and memory), where RMSE less than 3% is adopted to determine the acceptable results and RMSE less than 2% is applied to judge the good results.

As shown in Table 7, except for the first 3 measurement points, the difference of MCS/TH1D and measured data varies within ±25 ppm, and ten of them lie within ±10 ppm. However, comparing MCS/CTF to measured data, the difference is within ±25 ppm at all measured points except for the first 3 points. Nine of them are even within ±10 ppm. It can be concluded that both MCS/CTF and MCS/TH1D provide the acceptable CBC results (detector signal) at measurement conditions. However, MCS/CTF has better accuracy than MCS/TH1D, especially in the first 2 measurement points. This difference is caused by the fluid dynamic solutions with closed-channel model or sub-channel model [25]. The power level at BOC (beginning of cycle) should not be as flat as that in MOC (middle of cycle) and EOC (end of cycle), which introduces more significant cross-flow effects in CTF. However, this effect could not be considered in TH1D.

4.3.2. Radial detector signal distribution

Moreover, the MCS/CTF and MCS/TH1D simulated results of assembly-wise detector signal distribution were also collected and compared with measured data, as illustrated in Figs. 6–8. Note that although we compared MCS/TH1D with measured data, the detector signal distribution from MCS/TH1D is not directly displayed in the figures.

Table 8 lists the minimum ("MIN"), maximum ("MAX"), and root mean square ("RMS") relative errors for comparison at each burnup step of Cycle 2. Note that those relative errors are absolute values.

Considering the RMS of relative errors, the overall values for both MCS/CTF and MCS/TH1D lie in the range of 1.17%–3.11%, which is acceptable for the accuracy comparison. Only at Step 1, the RMS relative errors slightly exceed 4%. However, the difference between MCS/TH1D and MCS/CTF is not significant. At Steps 6,8,10,11 and 12, MCS/TH1D is slightly better than MCS/CTF, which is inversed at the remaining steps.

4.3.3. Axial detector signal distribution

The quarter core integrated axial detector signals from MCS/CTF simulated results was compared to MSC/TH1D and measured data at BOC, MOC and EOC of BEAVRS Cycle 2 depletion.

It can be seen from Figs. 9–11 that CTF is capable of producing considerably accurate results as TH1D in the case of BOC, MOC and EOC, when quarter core axial signals distributions are quite flat. All of them calculated from MCS/CTF and MCS/TH1D have acceptable accuracy compared to the measured data.

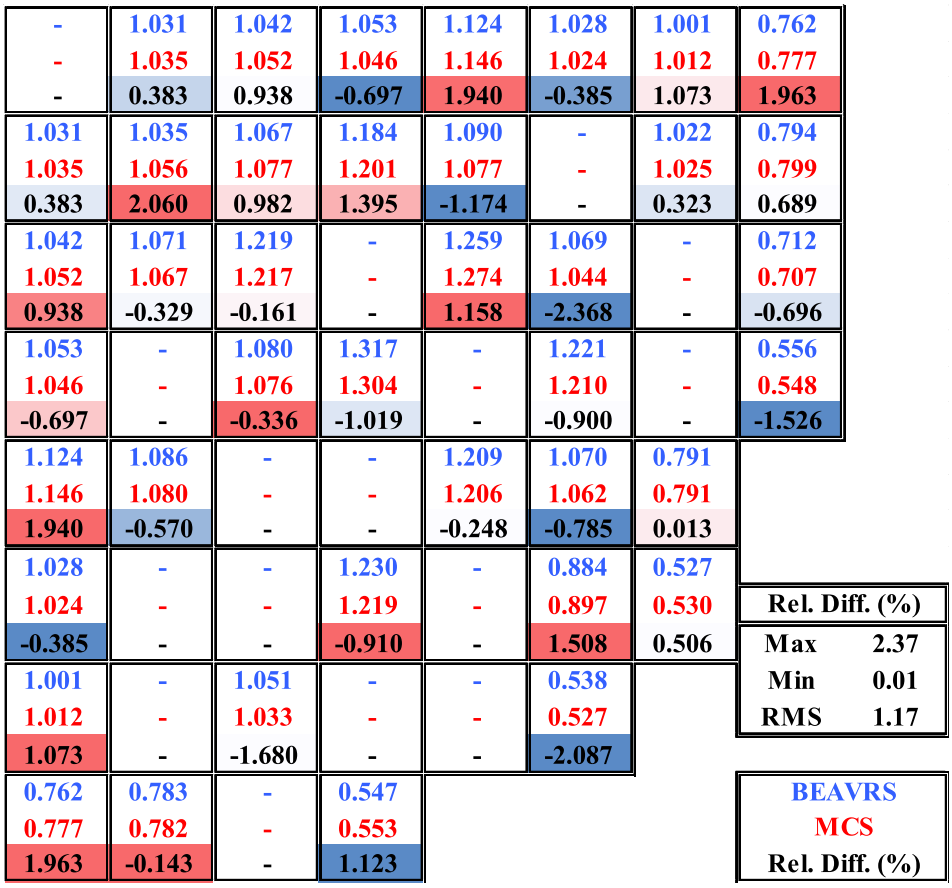

Fig. 8. Assembly-wise detector signals distribution at EOC of Cycle 2 (Step 14).

Table 8
Relative error between MCS/CTF and MCS/TH1D at all burnup steps.

Step	EFPD [days]	MIN [%]		MAX [%]		RMS [%]	
		TH1D	CTF	TH1D	CTF	TH1D	CTF
1	0.31	0.40	0.11	10.43	10.82	5.47	4.08
2	3.01	0.04	0.08	7.16	6.01	2.87	2.43
3	5.39	0.17	0.20	5.21	5.43	3.10	2.90
4	27.02	0.03	0.04	6.37	6.21	2.94	3.10
5	33.48	0.06	0.27	13.10	5.47	4.05	2.99
6	50.19	0.31	0.21	5.13	5.74	2.68	2.90
7	76.05	0.33	0.12	5.54	5.36	3.00	2.70
8	96.13	0.04	0.09	5.57	6.31	2.57	2.65
9	124.25	0.12	0.01	5.07	4.43	1.58	1.47
10	155.09	0.08	0.08	5.15	5.04	2.27	2.59
11	183.43	0.12	0.14	6.87	7.33	2.76	3.03
12	207.55	0.05	0.07	6.71	5.43	2.50	2.81
13	222.47	0.24	0.19	8.43	6.77	3.28	3.11
14	248.06	0.17	0.01	6.71	2.37	3.03	1.17

Table 9 further lists the minimum ("MIN"), maximum ("MAX") and root mean square ("RMS") of relative difference compared to the measured detector signals at BOC, MOC and EOC. Those results are collected from the tallies of 60 equal-length axial meshes in MCS simulations. Note that the relative differences in Table 9 are nominal values instead of absolute values.

4.4. Comparison with TH1D

In the following figures (Figs. 12–14), the axially integrated distributions at BOC, MOC and EOC for power, fuel temperature, coolant temperature and coolant density are displayed from MCS/CTF simulated results. Their relative discrepancies from MCS/TH1D is also illustrated.

As displayed in Figs. 12–14, the axially integrated power distributions of BEAVRS quarter core simulation become flatter with the increase of burnup. Unlike the power distribution of Cycle 1 depletion results, the location of power peak moves from only-one assembly [5,6] to 7-assembly area, which is colored dark red in the figures. On the other hand, the relative difference between MCS/CTF and MCS/TH1D results does not significantly change from BOC to EOC, and their values range from approximately −5%–5%.

Figs. 15–17 present the fuel temperature distributions of the Cycle 2 quarter core simulation at BOC, MOC and EOC respectively. The fuel temperature distribution trends tightly toward the change of power distributions. The fuel temperature peaks are located in the 7-assembly area (colored dark red in the figures), as are the power peaks. On the other hand, the relative difference between MCS/CTF and MCS/TH1D ranges from approximately 1%–5%.

The distributions for some important T/H quantities, for instance, coolant temperature and coolant density, are presented in the following figures (Figs. 18–23). As shown in Figs. 18–20, the coolant temperature level increases with the increase of burnup. However, the distribution shape does not change a lot. Unlike the fuel temperature and power distribution, there is no clear border between neighbouring fuel assemblies, which is physically reasonable in the real reactor cores. This phenomenon can be seen only from the MCS/CTF results, since CTF solver is able to consider the cross-flow effect between neighbouring assemblies. On the other hand, the relative difference between MCS/CTF and MCS/

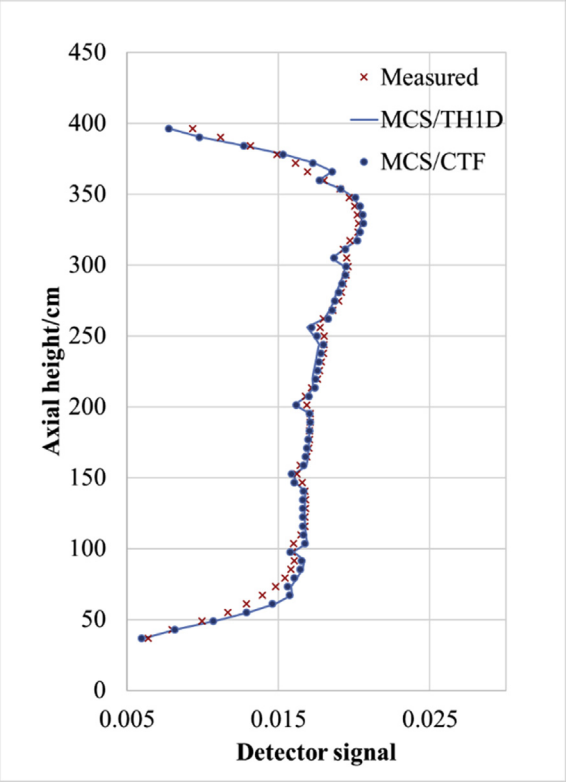

Fig. 9. Comparison of axial detector signals at BOC of Cycle 2 (Step 3).

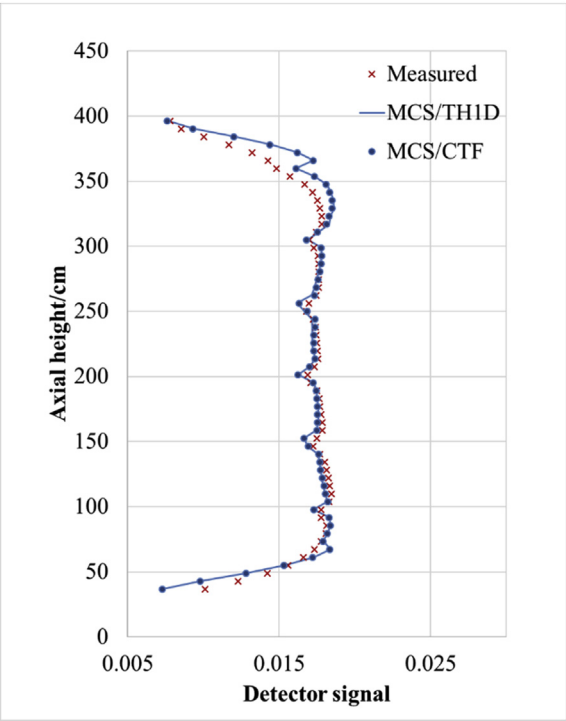

Fig. 10. Comparison of axial detector signals at MOC of Cycle 2 (Step 9).

TH1D results lies in the fuel assembly borders. The maximum relative error is around 0.5% regardless at BOC, MOC and EOC.

It can be seen from Figs. 21–23 that coolant density has a similar behavior to coolant temperature. Only the values in the area with

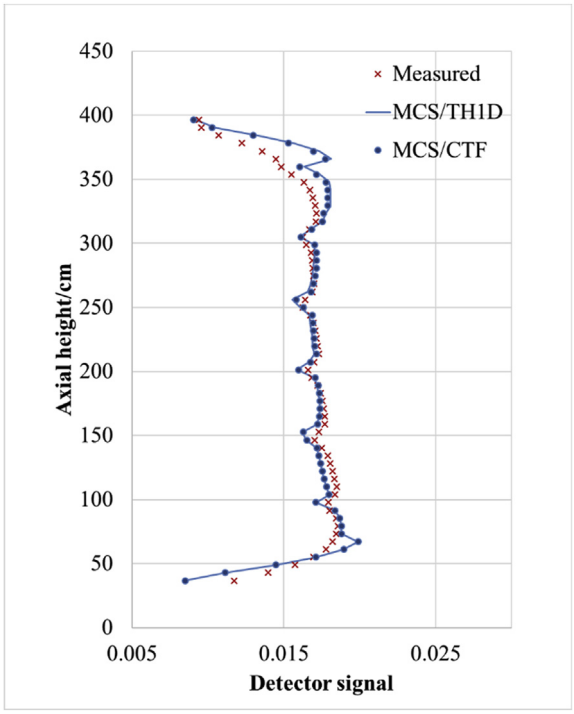

Fig. 11. Comparison of axial detector signals at EOC of Cycle 2 (Step 14).

Table 9
Relative difference of axial detector signals of Cycle 2.

Step	MIN [%]		MAX [%]		RMS [%]	
	TH1D	CTF	TH1D	CTF	TH1D	CTF
3	−30.80	−30.47	36.28	34.05	9.27	8.78
9	−10.58	−11.11	16.24	16.20	3.45	3.46
14	−23.73	−20.55	20.87	15.06	5.20	4.49

the highest power level changed visually. And again, no clear border can be recognized from the distribution at the connection area of neighbouring fuel assemblies. On the other hand, the big relative differences between MCS/CTF and MCS/TH1D also exist in the border area of neighbouring fuel assemblies. However, the values of relative difference range from around −1.0% to 1.0% at BOC, MOC and EOC.

Furthermore, the difference of pin-power between MCS/TH1D and MCS/CTF reaches approximately 4% just as shown in Fig. 12. However, the difference of moderator temperature is much less (less than 0.5%). Although independent simulations with different random number seed have not carried out in this paper, in the MCS/CTF/FRAPCON coupling system application of BEAVRS Cycle 1 BOC HFP, the 25 independent simulations have been finished and analyzed [6]. The results show that the statistical uncertainties of radially integrated axial distributions reach 1%. But in the hottest fuel pin, the single pin has the uncertainty ranging from 1% to 5%. The calculation parameter in this paper were chosen according to the previous experience. Hence, the maximum pin-wise relative difference in Fig. 12 is approximately 4%, which value is very close to the maximum statistical uncertainty. And similarly, according to those results, the fuel temperature uncertainty significantly depends on power uncertainty. However, the coolant temperature and density have much smaller uncertainties, around 0.5%. The phenomenon observed from Figs. 12–23 is consistent with those in the reference [6], and acceptable in the quarter-core pin-wise

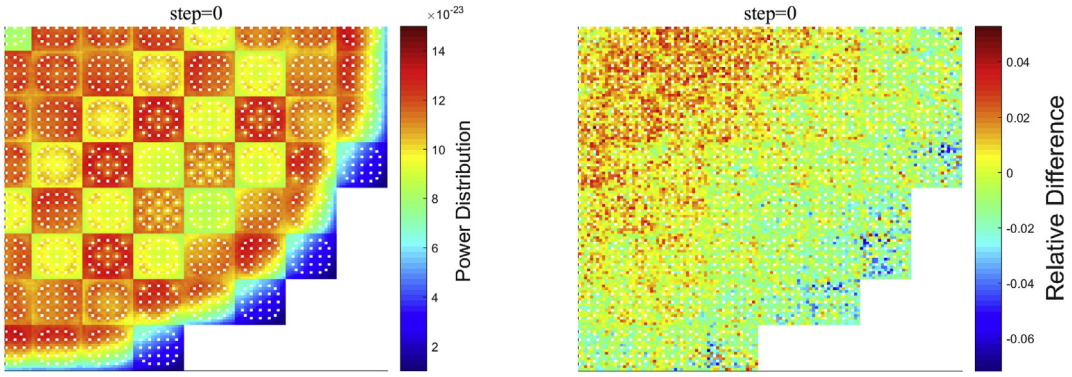

Fig. 12. Power distribution from MCS/CTF at BOC and the relative difference compared to MCS/TH1D.

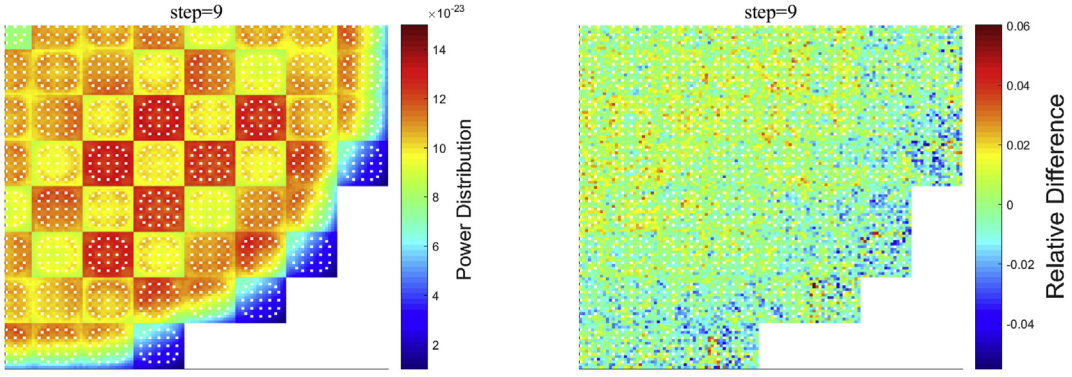

Fig. 13. Power distribution from MCS/CTF at MOC and the relative difference compared to MCS/TH1D.

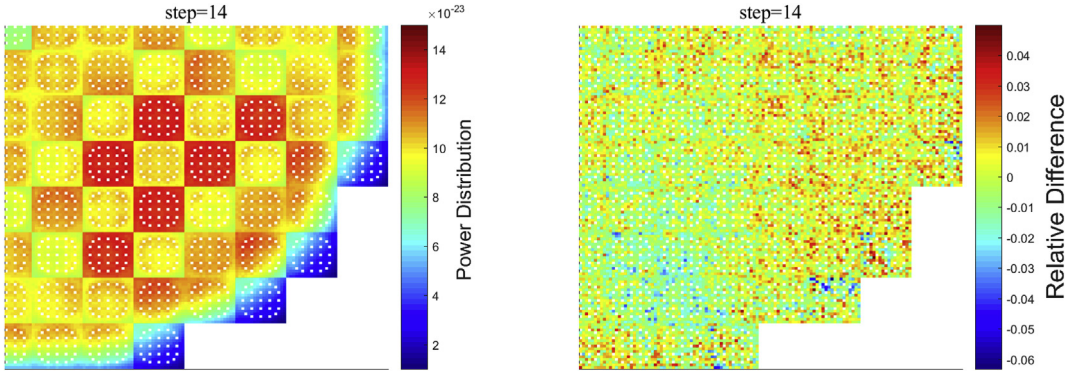

Fig. 14. Power distribution from MCS/CTF at EOC and the relative difference compared to MCS/TH1D.

depletion simulation with T/H feedback based on the current computational tools and resources.

5. Conclusions

The quarter-core model of BEAVRS Benchmark Cycle 2 depletion with T/H feedback was performed using Monte Carlo based multi-physics coupling code system MCS/CTF and MCS/TH1D. Other than RMC, there have been no other Monte Carlo results published for BEAVRS Cycle 2 full core depletion. Therefore, this paper only focuses on the comparison of MCS simulated results and measured data, including boron letdown with the whole fuel cycle, CBC detector signal at realistic core operating condition and the corresponding assembly-wise detector signal distributions. Firstly, the detailed computation time was compared between MCS/CTF and MCS/TH1D. And the time ratio results show that MCS/CTF consumes averaged 22% additional time than MCS/TH1D, which is reasonable because of the more complicated sub-channel fluid dynamic being applied in CTF. Then, boron letdown with 100% power level during the full cycle has also been compared with the measured data. The CBC difference shows good agreement between MCS results (including MCS/CTF and MCS/TH1D) and measurement, although the power level (100% HFP) at MCS depletion simulation is different from that in boron letdown measurement. Additionally, detector signal CBC and assembly-wise flux distribution at real measurement conditions at each burnup step were simulated by MCS/CTF and MCS/TH1D respectively. The CBC comparison results show that the differences lie in the range of ±25 ppm except for the first three points at BOC. The similar phenomenon is observed for both MCS/CTF and MCS/TH1D results. It

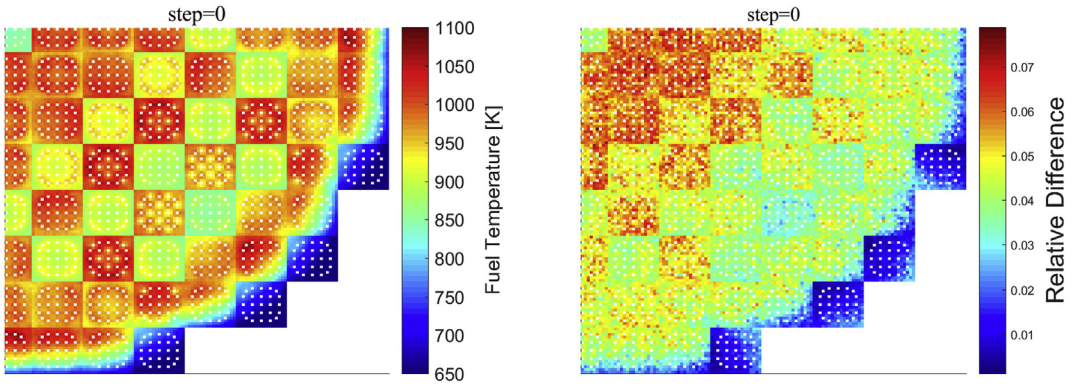

Fig. 15. Fuel temperature distribution from MCS/CTF at BOC and the relative difference compared to MCS/TH1D.

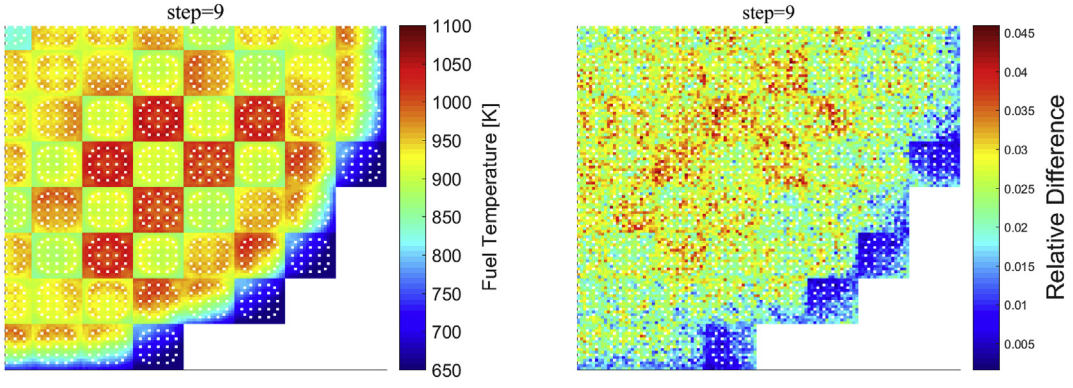

Fig. 16. Fuel temperature distribution from MCS/CTF at MOC and the relative difference compared to MCS/TH1D.

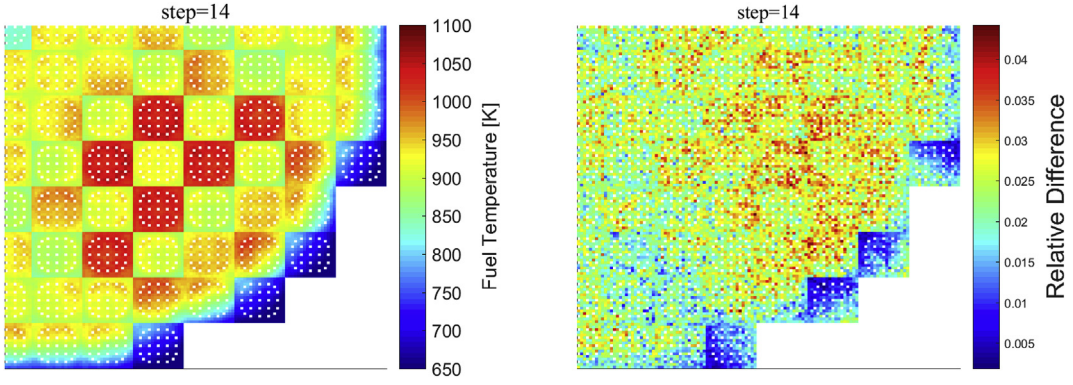

Fig. 17. Fuel temperature distribution from MCS/CTF at EOC and the relative difference compared to MCS/TH1D.

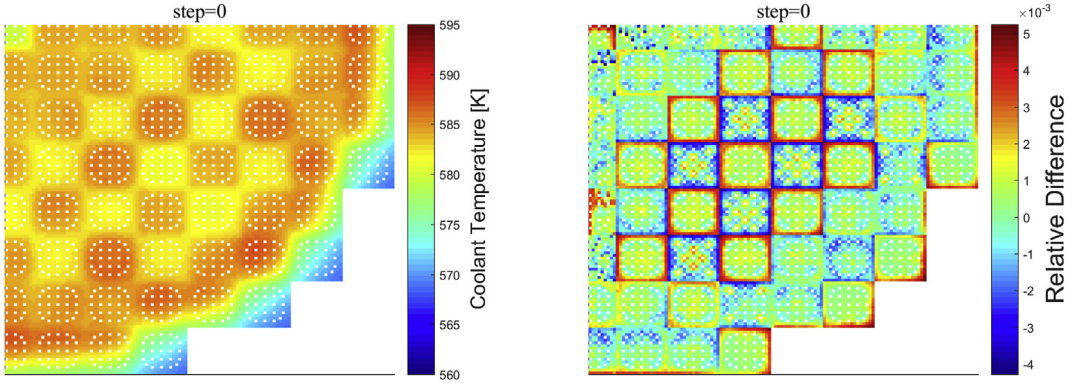

Fig. 18. Coolant temperature distribution from MCS/CTF at BOC and the relative difference compared to MCS/TH1D.

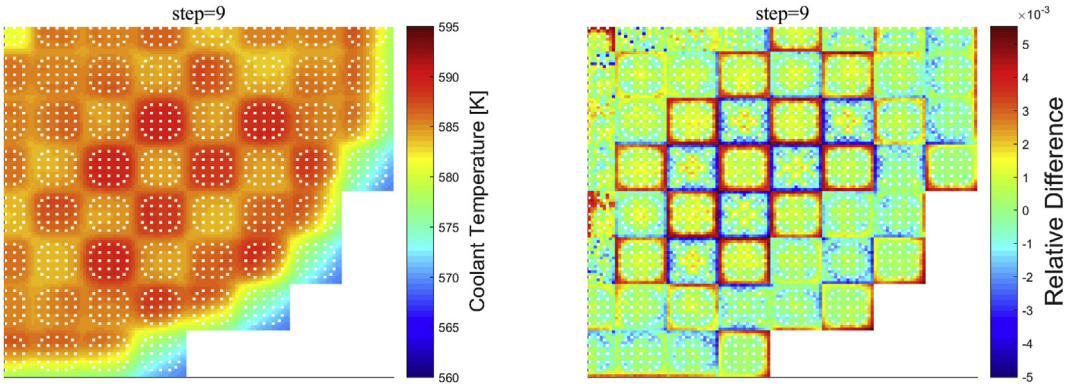

Fig. 19. Coolant temperature distribution from MCS/CTF at MOC and the relative difference compared to MCS/TH1D.

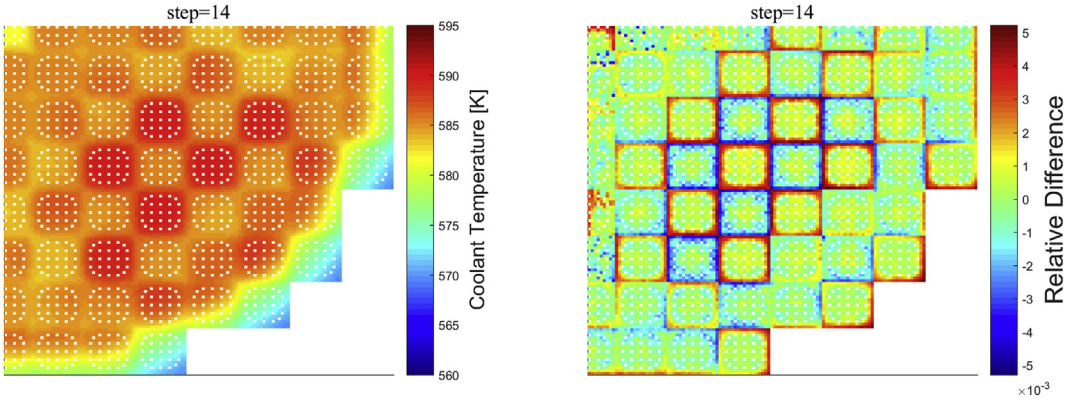

Fig. 20. Coolant temperature distribution from MCS/CTF at EOC and the relative difference compared to MCS/TH1D.

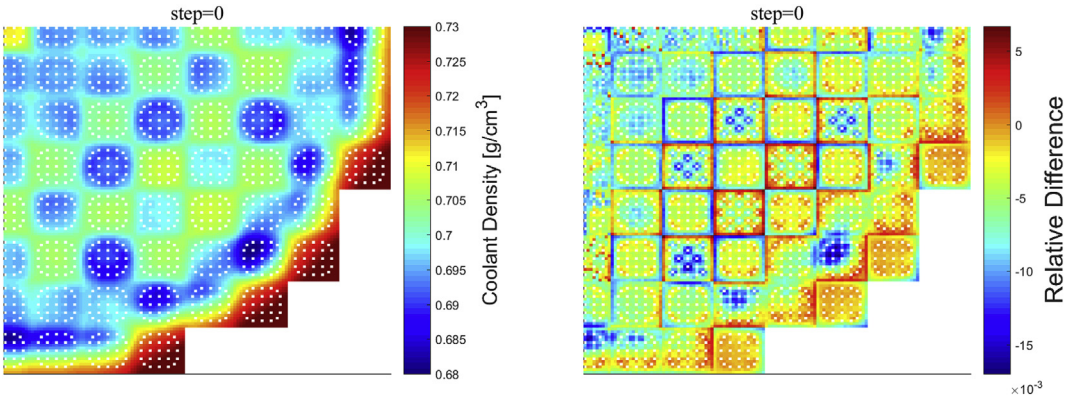

Fig. 21. Coolant density distribution from MCS/CTF at BOC and the relative difference compared to MCS/TH1D.

proves that MCS/CTF and MCS/TH1D can provide CBC results with considerably the same accuracy. The assembly-wise flux distribution comparison also illustrates good agreement between measurement data and simulation results. In addition, the calculated quarter-core axial power distributions are also presented and compared to the measured data. From the view point of relative difference, MCS/CTF wins MCS/TH1D by a narrow margin. However, axial power distributions get converged for both MCS/CTF and MCS/TH1D. Finally, the detailed axially-integrated radial distributions, including power density, fuel temperature, coolant temperature and coolant density at BOC, MOC and EOC were presented and analyzed to show the differences between MCS/CTF and MCS/TH1D. The comparison results prove that CTF is better to be coupled as the T/H solver, which is capable of obtaining more detailed and more reasonable distributions with cross-flow effect between neighbouring sub-channels.

However, certain limitations exist in this work as follows: the quarter-core symmetry is approximated in the modelling; the neutronic mesh (especially for fuel pellets) is not good enough for high fidelity simulations. Those drawbacks should be improved in the future work. In addition, the higher order coupling schemes, e.g., JFNK (Jacobian-Free Newton-Krylov), might be developed in MCS and coupled T/H solvers. Further analysis and comparative study will also be conducted on the sensitivity analysis and

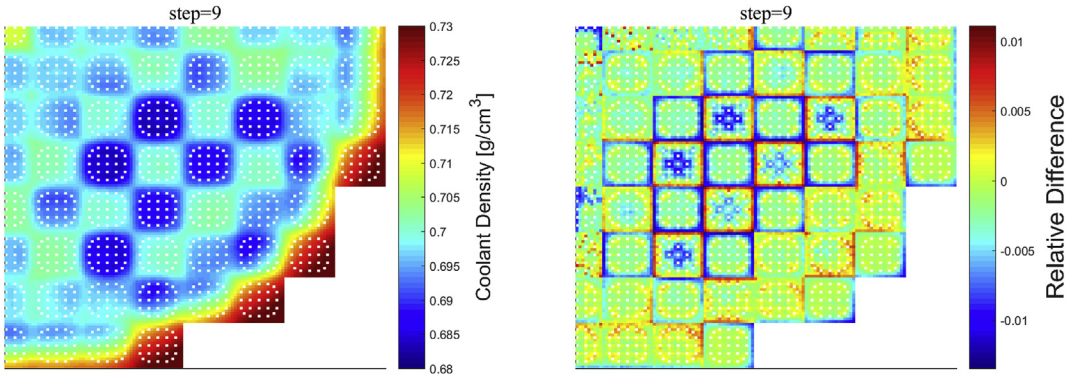

Fig. 22. Coolant density distribution from MCS/CTF at BOC and the relative difference compared to MCS/TH1D.

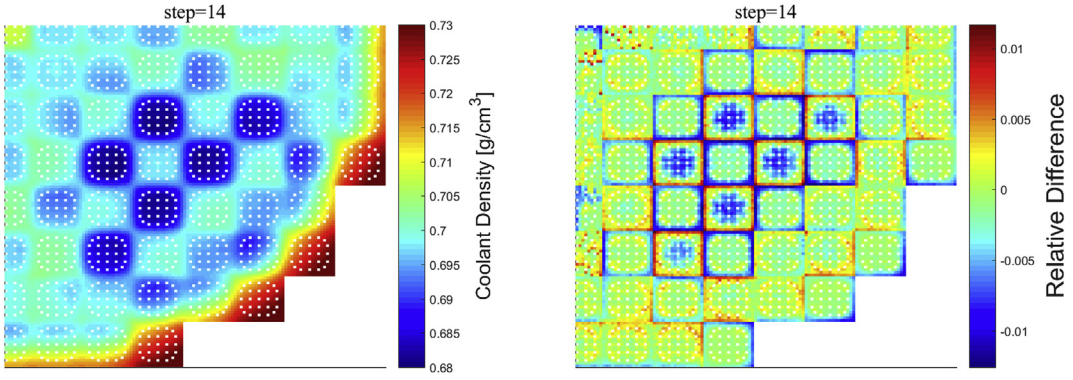

Fig. 23. Coolant density distribution from MCS/CTF at BOC and the relative difference compared to MCS/TH1D.

uncertainty quantification of the multi-physics coupling simulation.

Acknowledgements

This research was supported partially by the National Research Foundation of Korea (NRF) grant funded by the Korean government (MSIT) (No. 2017M2B2A9A02049916), and partially by the project (L17S018000) funded by Korea Hydro & Nuclear Power Co. Ltd.

Appendix B. Supplementary data

Supplementary data to this article can be found online at https://doi.org/10.1016/j.net.2019.09.007.

Appendix A

Taking a 7-by-7 mini core (quarter core) as an example (with assemblies consisting of 3-by-3 fuel pins), Tables 1–1, 1-2, and 1-3 display the initial loading pattern of Cycle 1, the refueled loading pattern of Cycle 2 and the assembly clockwise rotation angles of Cycle 2 respectively.

Tables 1–1
Loading pattern of Cycle 1 for mini core

A01	A02		
B01	B02	B03	
C01	C02	C03	C04
D01	D02	D03	D04

Tables 1–2
Loading pattern of Cycle 2 for mini core

NEW	D01		
D03	NEW	D02	
C02	C01	NEW	B03
C04	B01	A02	NEW

Tables 1–3
Rotation angle of Cycle 2 for mini core

0	90		
270	0	180	
0	180	0	90
90	0	270	0

I.1 MCS index

The left-hand figure in Fig. I-1 displays the MCS index numbering of fuel pins at Cycle 1, which is simply based on fuel pin numbering (guide tubes are excluded) starting from bottom left to top right in both assembly and core levels. However, as shown in the right-hand figure of fuel pin indexing in Cycle 2, the order of assembly wise indexing is still starting from bottom left to top right. Due to the rotation, the indexing inside each assembly changes according to the clockwise angle.

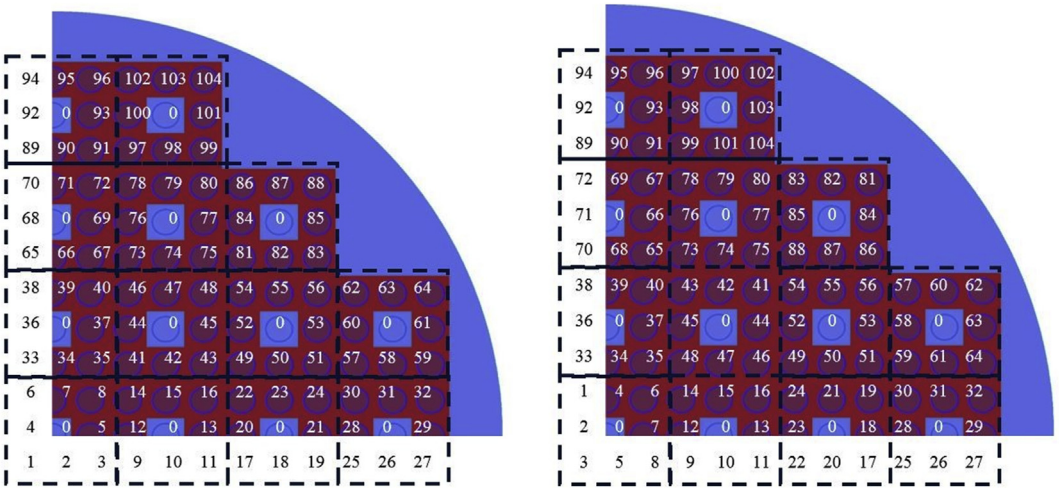

Fig. 1–. 1Index of fuel pins in Cycle 1 (left) and Cycle 2 (right) with rotation

I.2. Fuel pin index at T/H solvers

TH1D is a one-dimension T/H solver, all the data transferred can be easily classified by each single pin. Therefore, the fuel pin index in TH1D is set to be absolutely the same as that in the MCS index, in both the initial and refueled loading patterns. The CTF index of fuel pins in Cycle 1 and 2 are consistent just as shown in Fig. I-2, where the fuel rods and guide tubes are globally numbered from bottom left to top right in the case of quarter core.

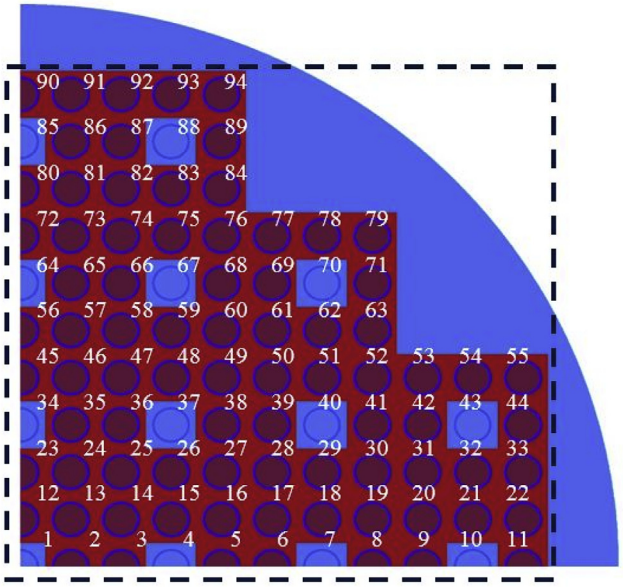

Fig. 1–2. CTF index of fuel pins in Cycle 1 and Cycle 2

References

[1] H.S. Lee, W.Y. Kim, P. Zhang, et al., Development Status of Monte Carlo Code at UNIST, KNS 2016 Spring Meeting, Jeju, Korea, 2016. May 12-13.

[2] R.K. Salko, CTF Theory Manual, Reactor Dynamics and Fuel Management Group, Pennsylvania State University, 2014.

[3] K.J. Geelhood, W.G. Luscher, FRAPCON-4.0: Integral Assessment, Pacific Northwest National Laboratory, 2015. PNNL-19418.

[4] J. Yu, H. Lee, H. Kim, et al., Preliminary validation of MCS multi-physics coupling capability with CTF, in: Proceedings of the Reactor Physics Asia 2017 (RPHA17) Conference, Chengdu, China, 2017. August. 24-25.

[5] J. Yu, S. Lee, D. Lee, Fuel Performance Coupling of FRAPCON within MCS, Transactions of 2017 ANS Winter Meeting, Washington, D.C., 2017. Oct. 29-Nov. 2.

[6] J. Yu, H. Lee, M. Lemaire, et al., MCS based neutronics/thermal-hydraulics/fuel-performance coupling with CTF and FRAPCON, Comput. Phys. Commun. 238 (2019) 1–18.

[7] CASL, Consortium for advanced simulation of light water reactors (CASL). http://www.casl.gov/, 2015.

[8] S.C. Benjamin, G. Andrew, S. Shane, et al., Simulation of the BEAVRS Benchmark Using VERA, M&C 2017 – International Conference on Mathematics & Computational Methods Applied to Nuclear Science & Engineering, 2017. Jeju, Korea, April 16-20.

[9] B. Kochunas, D. Jabaay, T. Downar, et al., Validation and Application of the 3D Neutron Transport MPACT within CASL VERA-CS, Oak Ridge National Laboratory, 2015.

[10] B. Kochunas, B. Collins, S. Stimpson, et al., VERA core simulator methodology for pressurized water reactor cycle depletion, Nucl. Sci. Eng. 185 (1) (2017) 217–231.

[11] J.A. Turner, K. Clarno, M. Sieger, et al., The virtual environment for reactor applications (VERA): design and architecture, J. Comput. Phys. 326 (2016) 544–568, 2016.

[12] B. Kochunas, B. Collins, D. Jabaay, et al., Overview of development and design of MPACT: Michigan parallel characteristics transport code, Proc. M C 2013 (May 5-9, 2013). Sun Valley, ID, USA.

[13] J.D. Hales, S.R. Novascone, B.W. Spencer, et al., Verification of the BISON fuel performance code, Ann. Nucl. Energy 71 (2014) 81–90.

[14] S. Liu, J. Liang, Q. Wu, et al., BEAVRS full core burnup calculation in hot full power condition by RMC code, Ann. Nucl. Energy 101 (2017) 434–446.

[15] S. Liu, J. Yu, J. Liang, et al., Study of neutronics and thermal-hydraulics coupling with RMC COBRA-EN system, in: 7th International Conference on Modelling and Simulation in Nuclear Science and Engineering (7ICMSNSE), Ottawa, Ontario, Canada, 2015. October 18–21.

[16] J. Guo, S. Liu, X. Shang, et al., Coupled neutronics/thermal-hydraulics analysis of a full PWR core using RMC and CTF, Ann. Nucl. Energy 109 (2017) 327–336.

[17] K. Wang, S. Liu, Z. Li, et al., Analysis of BEAVRS two-cycle benchmark using RMC based on full core detailed model, Prog. Nucl. Energy 98 (2017) 301–312.

[18] K. Li, S. Liu, J. Guo, et al., Up-to-Date Results of BEAVRS Two-Cycle Benchmark with Internal Coupling between RMC and CTF, Transactions of 2018 ANS Winter Meeting, Nov.11-15, 2018. Orlando, FL.

[19] H.S. Lee, W.K. Kim, P. Zhang, et al., Preliminary Simulation Results of BEAVRS Three-Dimensional Cycle 1 Wholecore Depletion by UNIST Monte Carlo Code MCS, M&C 2017 – International Conference on Mathematics and Computational Methods Applied to Nuclear Science and Engineering, 2017. Jeju, Korea, April 16-20, 2017.

[20] N. Horelik, B. Herman, B. Forget, et al., Benchmark for evaluation and validation of reactor simulations (BEAVRS), v1. 0.1, in: Proc. Int. Conf. Mathematics and Computational Methods Applied to Nuc. Sci. & Eng., 2013.

[21] N. Horelik, MIT Benchmark for Evaluation and Validation of Reactor Simulations (BEAVRS), Version 2.0, MIT Computational Reactor Physics Group, Massachusetts Institute of Technology, 2016.

[22] N. Horelik, MIT Benchmark for Evaluation and Validation of Reactor Simulations (BEAVRS), Rev. 2.0.2, MIT Computational Reactor Physics Group, Massachusetts Institute of Technology, 2018.

[23] D.J. Kelly, T.M. Sutton, S.C. Wilson, MC21 analysis of the nuclear energy agency Monte Carlo performance benchmark problem, Proc. PHYSOR Adv React. Phys. Link. Res., Ind. Educ. (2012) 15–20.

[24] K. Smith, B. Forget, Challenges in the development of high-fidelity LWR core neutronics tools, in: International Conference on Mathematics and Computational Methods Applied to Nuclear Science and Engineering (M&C2013), Sun Valley, Idaho, USA, 2013. May 5-9.

[25] A. Yamamoto, I. Tsutomu, Impact of pin-by-pin thermal-hydraulic feedback modeling on steady-state core characteristics, Nucl. Technol. 149 (2) (2005) 175–188.